Adaptive Thyristor-Controlled LC-Hybrid Active Power Filter for Reactive Power and Current Harmonics Compensation With Switching Loss Reduction

Chi-Seng Lam, *Senior Member, IEEE*, Lei Wang, Sut-Ian Ho, and Man-Chung Wong, *Senior Member, IEEE*

***Abstract*—In this paper, an adaptive dc-link voltage controlled thyristor-controlled LC-coupling hybrid active power filter (TCLC-HAPF) is proposed for reducing switching loss, switching noise, and enhancing the compensating performance. Unfortunately, the TCLC-HAPF has both controllable active TCLC part and active inverter part; thus, the conventional minimum dc-link voltage calculation methods for active power filter (APF) and LC-coupling hybrid APF (LC-HAPF) cannot be directly applied to the TCLC-HAPF. Moreover, the aforementioned dc-link voltage calculation methods were developed based on the fast Fourier transform (FFT), which makes the calculation complex. This paper also presents a simplified minimum dc-link voltage calculation method for TCLC-HAPF reactive power and current harmonics compensation, which can significantly reduce the large amount of the calculation steps by using the FFT method. After that, an adaptive dc-link voltage controller for the TCLC-HAPF is developed to dynamically keep its operating at its minimum dc-link voltage level to reduce its switching loss and switching noise. Finally, representative simulation and experimental results are given to verify the proposed simplified dc-link voltage calculation method and the adaptive dc-link voltage control method of TCLC-HAPF.**

***Index Terms*—Adaptive dc-link voltage control, current harmonics, reactive power, thyristor-controlled LC-hybrid active power filter (TCLC-HAPF).**

I. Introduction

With the proliferation and increased use of power electronics devices (nonlinear loads) and motor loadings, such as converters, adjustable speed drives, arc furnaces, bulk rectifiers, power supplies, computers, fluorescent lamps, elevators, escalators, large air conditioning systems, compressors, etc., in distribution power systems, the power quality (PQ) problems become more serious, especially for lower power factor and harmonic pollution [1]–[11]. To solve the above PQ issues, different PQ compensators have been developed.

The active power filters (APFs) have been widely used to dynamically compensate reactive power and harmonic current. However, the APFs require high dc-link voltage (V_{dc}) for performing compensation, so their initial and operating costs are high [5]–[11]. Afterwards, different hybrid APF (HAPF) topologies composed of APF and passive power filter (PPF) in series and/or parallel have been proposed [4]–[9], aiming to improve the compensation characteristics of PPFs and reduce the voltage and/or current ratings (costs) of the APFs. LC-coupled HAPFs (LC-HAPFs) [12]–[16] can be considered as a good tradeoff between the system cost and compensation performance, which aims to reduce the dc-link operating voltage. However, the LC-HAPF has a narrow reactive power variation range, which may require a high V_{dc} when it is operating outside its compensation range, thus losing its low V_{dc} characteristic. To enlarge the compensation range and keep at a low rating of active inverter part simultaneously, a thyristor-controlled LC-coupling-hybrid APFs (TCLC-HAPFs) were proposed in 2014 and 2016 for distribution [17], [18] and transmission power systems [19], respectively. The TCLC-HAPF can provide a much wider reactive power compensation range than the LC-HAPF and keeps the low dc-link operating voltage characteristics as the LC-HAPF.

In practical case, there is always a minimum dc-link voltage for PQ compensators performing load reactive power and harmonic current compensation. As the switching loss is directly proportional to V_{dc} [14], [16], [20], the PQ compensators have higher switching loss if V_{dc} is higher, and vice versa. On the other hand, a sufficient V_{dc} can ensure satisfactory compensation performance. Thus, it is necessary to obtain an appropriate V_{dc} to achieve satisfactory compensation performance with low switching loss and switching noise.

Different minimum V_{dc} design methods for different PQ compensators have been reported among the existing literature [14]–[16], [21]–[24]. In [22]–[24], V_{dc} of the APFs are designed to be equal or larger than certain voltage levels, such as line to line voltage peak value [22], $2\sqrt{2}$ times the fundamental output

Manuscript received October 20, 2016; revised December 5, 2016; accepted December 11, 2016. Date of publication December 15, 2016; date of current version May 9, 2017. This work was supported in part by the Macau Science and Technology Development Fund (FDCT 109/2013/A3) and in part by the Research Committee of the University of Macau (MYRG2015-00030-AMSV MYRG2015-00009-FST, MRG012/WMC/2015/FST). Recommended for publication by Associate Editor Khai Ngo. *(Corresponding author: C.-S. Lam).*

C.-S. Lam is with the State Key Laboratory of Analog and Mixed Signal VLSI, University of Macau, Macao, China (e-mail: cslam@umac.mo).

L. Wang is with the Department of Electrical and Computer Engineering, Faculty of Science and Technology, University of Macau, Macao, China.

S.-I. Ho and M.-C. Wong are with the State Key Laboratory of Analog and Mixed Signal VLSI and the Department of Electrical and Computer Engineering, Faculty of Science and Technology, University of Macau, Macao, China.

Color versions of one or more of the figures in this paper are available online at http://ieeexplore.ieee.org.

Digital Object Identifier 10.1109/TPEL.2016.2640304

voltage of the active inverter [23], $2\sqrt{2}$ times the root mean square (rms) value of the system source voltage [24]. However, the $V_{\rm dc}$ calculation methods in [22]–[24] are not related to the loading situation, so that the calculated $V_{\rm dc}$ are not accurate for compensation. To obtain a more accurate $V_{\rm dc}$ requirement for APF, Lam *et al*. [21] proposed a detailed deduction analysis of the minimum $V_{\rm dc}$ value for both fundamental reactive power and current harmonic compensation based on the complicated fast Fourier transform (FFT). Later on, the minimum $V_{\rm dc}$ calculation method of APF has been extended to the LC-HAPF systems [14]–[16]. Even through the $V_{\rm dc}$ calculation method for the adaptive $V_{\rm dc}$-controlled LC-HAPF in [14] is based on the single-phase instantaneous p–q theory [25], the work in [14] aims to compensate dynamic reactive power problem only without current harmonics consideration. When the LC-HAPFs are designed to compensate both reactive power and current harmonics simultaneously, similar as APF case, the $V_{\rm dc}$ calculation still requires the FFT [15], [16], which makes the $V_{\rm dc}$ calculation complex. As the TCLC-HAPF has controllable active TCLC part and active inverter part, it should have different $V_{\rm dc}$ calculation equations in comparison to the APFs and the LC-HAPFs as they have fixed passive *L*/*LC* part.

Even though TCLC-HAPF was first proposed in 2014 [17], the derivation of its $V_{\rm dc}$ design was reported in [18]. However, $V_{\rm dc}$ in [18] was proposed to compensate the fundamental reactive power left by the TCLC part, while the current harmonic components and the loading reactive power over the TCLC part compensation range situation have not been taken into consideration. If the $V_{\rm dc}$ design in [18] is directly applied to compensate time-varying nonlinear loads, the TCLC-HAPF may fail to perform satisfactory current quality compensation.

Moreover, the TCLC-HAPF is always operating at a fixed $V_{\rm dc}$ level [17]–[19], the TCLC-HAPF will obtain a larger switching loss if a higher $V_{\rm dc}$ is used, and vice versa. Therefore, if $V_{\rm dc}$ can be adaptively changed according to different loading situations, the TCLC-HAPF can achieve better performances and operational flexibility. Besides, if the $V_{\rm dc}$ calculation for the TCLC-HAPF is based on the instantaneous p–q theory instead of using the complicated FFT as in [15], [16], and [21], the number of $V_{\rm dc}$ calculation steps and its corresponding processing time can be significantly reduced, which can relax the original complex $V_{\rm dc}$ calculation problem. Due to the limitations among the existing literature, the contributions of this paper are as follows:

1) Propose a $V_{\rm dc}$ calculation method for the TCLC-HAPF, in which the proposed $V_{\rm dc}$ method in [14]–[16], and [21] for the APF or the LC-HAPF cannot be directly applied to the TCLC-HAPF because the TCLC-HAPF has controllable active TCLC part (which changes depending on the loading situation) and active inverter part, while the APFs and the LC-HAPFs have fixed passive L/LC part (which is independent of the loading situation).
2) Propose a simplified minimum $V_{\rm dc}$ calculation for the TCLC-HAPF reactive power and current harmonics compensation, which can significantly reduce the number of calculation steps compared to the conventional $V_{\rm dc}$ calculation methods based on the FFT [15], [16], [21]; thus, the digital controller can reduce the required processing time and ensure the system response time and performance.

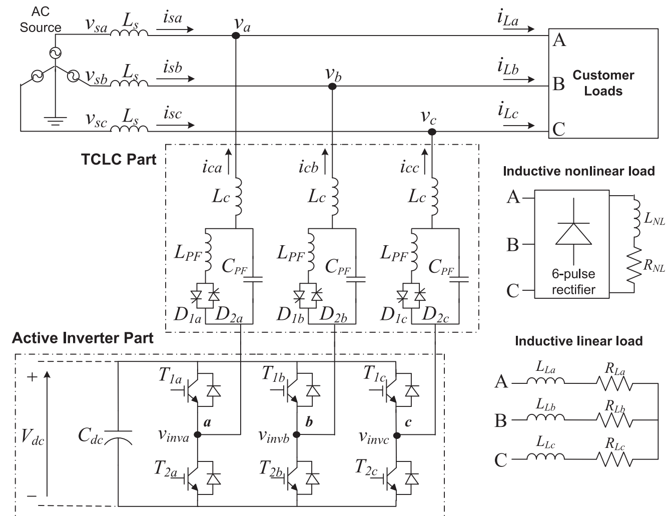

Fig. 1. Circuit configuration of a three-phase three-wire TCLC-HAPF.

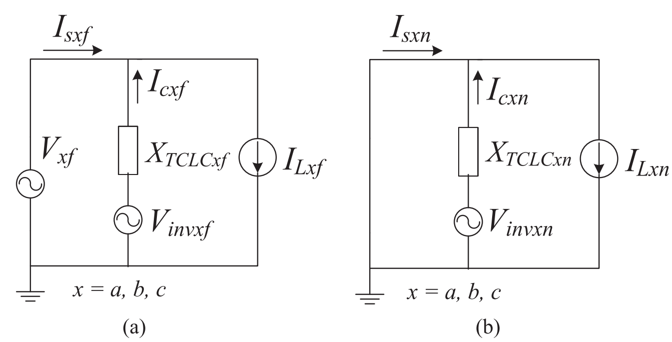

Fig. 2. Single-phase equivalent circuit models of the TCLC-HAPF: (a) at fundamental frequency, (b) at *n*th order harmonic frequency.

3) Develop an adaptive dc-link voltage controller for the TCLC-HAPF reactive power and current harmonics compensation based on the simplified $V_{\rm dc}$ calculation method, in which the proposed adaptive control can also be used for unbalanced loading compensation.
4) With the proposed adaptive dc-link voltage controller, the TCLC-HAPF can operate at its required $V_{\rm dc}$ level, thus lowering the system switching loss and noise.

In this paper, the background information and motivation of this paper are introduced in Section I. The circuit configuration and modeling of a three-phase three-wire TCLC-HAPF are described in Section II. Based on its modeling, the simplified $V_{\rm dc}$ calculation method is proposed in Section III and the adaptive $V_{\rm dc}$ control block is given in Section IV. Then, representative simulation case studies (in Section V) and experimental results (in Section VI) are provided to verify the deduced $V_{\rm dc}$ calculation method and the proposed adaptive $V_{\rm dc}$ controller for the TCLC-HAPF. Finally, conclusion is drawn in Section VII.

II. Circuit Configuration of Three-Phase Three-Wire TCLC-HAPF

The circuit configuration of a three-phase three-wire TCLC-HAPF is shown in Fig. 1. Fig. 2 shows the single-phase

TCLC-HAPF equivalent circuit models at the fundamental and harmonic frequencies. In this TCLC-HAPF topology, the TCLC part and the active inverter part can complement each other's disadvantages. As the TCLC part offers the reactive power compensation range and provides a large fundamental voltage drop between the load voltage and the active inverter voltage, the voltage rating of the active inverter part can be significantly reduced. On the other hand, the active inverter part can solve the inherent problems of using the TCLC alone, such as inrush currents, resonance problem, noise of thyristors turning on/off, mistuning of firing angles, and low harmonic compensation ability.

From Fig. 1, $v_{\rm sx}$, $i_{\rm sx}$, v_x, $i_{\rm Lx}$, and $i_{\rm cx}$ ("*x*" denotes phase *a*, *b*, or *c*) represent the source voltage, source current, load voltage, load current, and compensating current, respectively, L_s is the system inductance. For the TCLC part, L_c, $C_{\rm PF}$, and $L_{\rm PF}$ are its coupling inductor, parallel capacitor, and its thyristor-controlled reactor; and the pair of D_{1x} and D_{2x} is the bi-directional thyristor switch of the TCLC part. For the active inverter part, $v_{\rm invx}$ is the output voltage of the voltage source inverter (VSI); T_{1x} and T_{2x} are the switching devices; $C_{\rm dc}$ and $V_{\rm dc}$ are the dc-link capacitor and its voltage. Fig. 2 shows the single-phase equivalent circuit models of the TCLC-HAPF. In the following, the subscripts "*f*," "*h*," and "*n*" represent the fundamental, total harmonic, and harmonic order.

For the fundamental frequency circuit model as shown in Fig. 2(a), $V_{\rm xf}$ and $V_{\rm invxf}$ are the fundamental load and VSI voltages; $I_{\rm sxf}$, $I_{\rm cxf}$, and $I_{\rm Lxf}$ are the fundamental source, reactive compensating, and load currents, $X_{\rm TCLCxf}$ is the fundamental reactance of the TCLC part.

For the *n*th order harmonic frequency circuit model as shown in Fig. 2(b), $V_{\rm invxn}$ is the *n*th order harmonic output voltage of the VSI; $I_{\rm sxn}$, $I_{\rm cxn}$, and $I_{\rm Lxn}$ are the *n*th order harmonic system, compensating, and load currents, $X_{\rm TCLCxn}$ is the *n*th order harmonic reactance of the TCLC part, with the harmonic order nth $= 6k\pm1$th, $k = 1, 2 \ldots \infty$ for the three-phase three-wire system [26], [27].

From Figs. 1 and 2, the phase fundamental and harmonic reactance values of the TCLC part can be calculated as [19]

$$X_{\rm TCLCxf}(\alpha_x) = \frac{\pi X_{\rm LPFf} X_{\rm CPFf}}{X_{\rm CPFf}(2\pi - 2\alpha_x + \sin 2\alpha_x) - \pi X_{\rm LPFf}} + X_{\rm Lcf}$$

$$X_{\rm TCLCxn}(\alpha_x) = \frac{\pi X_{\rm LPFn} X_{\rm CPFn}}{X_{\rm CPFn}(2\pi - 2\alpha_x + \sin 2\alpha_x) - \pi X_{\rm LPFn}} + X_{\rm Lcn} \quad (1)$$

where $X_{\rm Lcf} = \omega L_c$, $X_{\rm LPFf} = \omega L_{\rm PF}$, $X_{\rm CPFf} = 1/(\omega C_{\rm PF})$; $X_{\rm Lcn} = n\omega L_c$, $X_{\rm LPFn} = n\omega L_{\rm PF}$, $X_{\rm CPFn} = 1/(n\omega C_{\rm PF})$, ω $(= 2\pi f)$ is the fundamental angular frequency. α_x is the phase firing angle of the thyristor switches, which can be obtained from the TCLC-HAPF controller and the detailed discussion of the TCLC-HAPF control will be presented in Section IV.

With the help of Fig. 2, the minimum dc-link voltage calculation for the TCLC-HAPF will be proposed and discussed in Section III. In the following analysis, $v_{\rm sx}$ and v_x as shown in Fig. 1 are assumed to be pure sinusoidal without harmonic components, that is $V_{\rm sx} = V_x = V_{\rm xf}$ [14], [21] for simplification, and all the parameters are in rms values.

III. Proposed Simplified Minimum DC-Link Voltage Calculation Method

To avoid using the complicated FFT method of the minimum $V_{\rm dc}$ calculation [15], [16], [21] for the TCLC-HAPF reactive power and current harmonics compensation, a simplified minimum $V_{\rm dc}$ calculation method is proposed. $V_{\rm dc}$ of the TCLC-HAPF includes both fundamental and harmonic components which can be expressed as

$$V_{\rm dcx} = \sqrt{{V_{\rm dcxf}}^2 + {V_{\rm dcxh}}^2} \quad (2)$$

$$V_{\rm dc} = \max\left(V_{\rm dca}, V_{\rm dcb}, V_{\rm dcc}\right) \quad (3)$$

where $V_{\rm dcxf}$ and $V_{\rm dcxh}$ are the required dc-link voltages for compensating fundamental reactive power and current harmonics of each phase. The final $V_{\rm dc}$ is calculated as the maximum value among the three phase values. In this section, $V_{\rm dcxf}$ and $V_{\rm dcxh}$ will be separately discussed in Sections III-A and III-B, and a comparison of the $V_{\rm dc}$ calculation for the TCLC-HAPF by using the conventional FFT method [15], [16], [21] and the proposed method will be discussed in Section III-C.

A. Deduction of DC-Link Voltage ($V_{\rm dcxf}$) at Fundamental Frequency

From Fig. 2(a), the phase fundamental inverter output voltage ($V_{\rm invxf}$) can be expressed as

$$V_{\rm invxf} = |V_x - |X_{\rm TCLCxf}(\alpha_x)| \cdot |I_{\rm cxf}|| \quad (4)$$

where V_x, $I_{\rm cxf}$, and $X_{\rm TCLCxf}(\alpha_x)$ are the fundamental load voltage, fundamental reactive compensating current, and TCLC part fundamental impedance, respectively. The reactive power ($Q_{\rm cx\_TCLCf}(\alpha_x)$) provided by the TCLC part and the load reactive power ($Q_{\rm Lxf}$) can be expressed as

$$Q_{\rm cx\_TCLCf}(\alpha_x) = \frac{{V_x}^2}{X_{\rm TCLCxf}(\alpha_x)} \quad (5)$$

$$Q_{\rm Lxf} = V_x \cdot I_{Lxfq} = V_x \cdot (-I_{\rm cxf}) \quad (6)$$

where $I_{\rm Lxfq}$ is the phase fundamental load reactive current and is equal to $-I_{\rm cxf}$ after the TCLC-HAPF compensation at ideal case. By combining (4)–(6), the required dc-link voltage ($V_{\rm dcxf}$) at the fundamental frequency can be expressed as

$$V_{\rm dcxf} = \sqrt{6} \times V_{\rm invxf} = \sqrt{6} \cdot V_x \left| \frac{|Q_{\rm Lxf}| - |Q_{\rm cx\_TCLCf}(\alpha_x)|}{Q_{\rm cx\_TCLCf}(\alpha_x)} \right|. \quad (7)$$

In (7), $Q_{\rm cx\_TCLCf}(\alpha_x)$ can also be expressed as

$$Q_{\rm cx\_TCLCf}(\alpha_x) = \frac{{V_x}^2}{\frac{\pi X_{\rm LPFf} X_{\rm CPFf}}{X_{\rm CPFf}(2\pi - 2\alpha_x + \sin 2\alpha_x) - \pi X_{\rm LPFf}} + X_{\rm Lcf}} \quad (8)$$

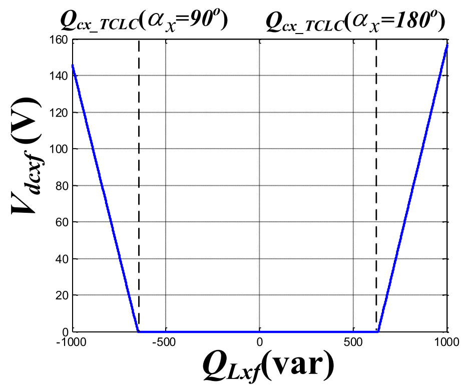

Fig. 3. Relationship between V_{dcxf} and Q_{Lxf}.

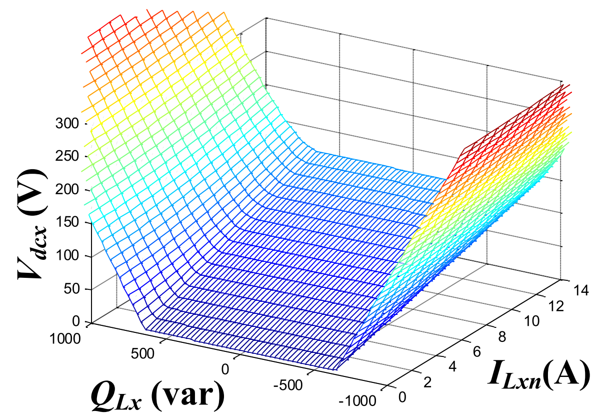

Fig. 4. Relationship among V_{dcx}, I_{Lxn}, and Q_{Lx}.

and it varies within two fixed boundaries according to the range $(90^\circ < \alpha_x < 180^\circ)$ of the firing angle as

$$Q_{\mathrm{cx\_TCLCf}}(\alpha_x = 90^\circ) = \frac{V_x^2}{X_{\mathrm{TCLCxf}}(\alpha_x = 90^\circ)} = \frac{V_x^2}{\frac{X_{\mathrm{LPFf}} X_{\mathrm{CPFf}}}{X_{\mathrm{CPFf}} - X_{\mathrm{LPFf}}} + X_{\mathrm{Lcf}}} \tag{9}$$

$$Q_{\mathrm{cx\_TCLCf}}(\alpha_x = 180^\circ) = \frac{V_x^2}{X_{\mathrm{TCLCxf}}(\alpha_x = 180^\circ)} = \frac{V_x^2}{X_{\mathrm{Lcf}} - X_{\mathrm{CPFf}}}. \tag{10}$$

Moreover, if Q_{Lxf} is within the compensation range of the TCLC part, that is $Q_{\mathrm{cx\_TCLCf}}(\alpha_x) = -Q_{\mathrm{Lxf}}$ and $V_{\mathrm{dcxf}} = 0$ can be achieved; otherwise, $V_{\mathrm{dcxf}} > 0$. Based on (7)–(10), the relationship between V_{dcxf} and Q_{Lxf} can be plotted as shown in Fig. 3.

B. Deduction of DC-Link Voltage (V_{dcxh}) at Harmonic Frequency

The three-phase three-wire nonlinear loads with six-pulse rectifiers such as ac–dc converters, speed-controlled dc motors, and steel hardening machines, etc., usually produce larger harmonic current than many other kinds of loads in the industrial applications [27]–[30]. Therefore, the six-pulse rectifier loads are mainly focused in this paper. If the proposed minimum V_{dc} can compensate this kind of rectifier loads, many other kinds of loadings can also be compensated [31], [32]. The harmonic currents (I_{Lxn}) of the six-pulse rectifier loads can be obtained through Fourier series [33] as

$$I_{\mathrm{Lxn}} = \frac{I_{\mathrm{Lxf}}}{n}, \quad n\mathrm{th} = 6k \pm 1\mathrm{th}, \quad k = 1, 2 \ldots \infty. \tag{11}$$

In (11), I_{Lxn} at each harmonic order can be expressed in terms of the fundamental load current (I_{Lxf}). Based on (11), the required dc-link voltage (V_{dcxh}) at harmonic frequency can be expressed as

$$V_{\mathrm{dcxh}} = \sqrt{6} \times \sqrt{\sum\nolimits_{n=2}^{\infty} \left(V_{\mathrm{invxn}}{}^2\right)} = \sqrt{6} \times \sqrt{\sum\nolimits_{n=2}^{\infty} \left[\left(X_{\mathrm{TCLCxn}}(\alpha_x) \times I_{\mathrm{Lxn}}\right)^2\right]} \tag{12}$$

$$V_{\mathrm{dcxh}} = \sqrt{6} \cdot I_{\mathrm{Lxf}} \cdot \sqrt{\sum\nolimits_{n=2}^{\infty} \left[\left(\frac{1}{n} \cdot X_{\mathrm{TCLCxn}}(\alpha_x)\right)^2\right]} = \sqrt{6} \cdot I_{\mathrm{Lxf}} \cdot A(\alpha_x) \tag{13}$$

where $A(\alpha_x) = \sqrt{\sum_{n=2}^{\infty} [(\frac{1}{n} \cdot X_{\mathrm{TCLCxn}}(\alpha_x))^2]}$.

In (13), $A(\alpha_x)$ is a constant related to $X_{\mathrm{TCLCxn}}(\alpha_x)$ and n, where $X_{\mathrm{TCLCxn}}(\alpha_x)$ is in terms of the firing angle (α_x) as shown in (1), and a look up table (LUT) (α_x vs $A(\alpha_x)$) can be built in order to simplify the $A(\alpha_x)$ calculation. Besides, the fundamental load current I_{Lxf} can be calculated by using the single-phase instantaneous p–q theory [25] as

$$S_{\mathrm{Lx}} = \frac{\sqrt{\bar{p}_{\mathrm{Lx}}^2 + \bar{q}_{\mathrm{Lx}}^2}}{2} \tag{14}$$

$$I_{\mathrm{Lxf}} = \frac{S_{\mathrm{Lx}}}{V_x} \tag{15}$$

where S_{Lx} is the apparent power of the loading, $\bar{p}_{\mathrm{Lx}}$ and $\bar{q}_{\mathrm{Lx}}$ are the dc components of the instantaneous load active and reactive power [25].

Based on the above deduction, from the TCLC-HAPF system parameters as shown in Table III, the phase required dc-link voltage V_{dcx} of the TCLC-HAPF can be plotted as shown in Fig. 4.

When there is no harmonic current problem, the required V_{dcx} will obtain the same results as shown in Fig. 3. The minimum $V_{\mathrm{dcx}} = 0$ can be achieved if Q_{Lx} is within the compensation range of the TCLC part. In addition, the larger the harmonic current contents, the larger the V_{dcx} requirement.

TABLE I
REQUIRED NUMBER OF MATHEMATICAL OPERATORS FOR THE CONVENTIONAL MINIMUM V_{dcx} CALCULATION BY USING FFT [15], [16], [21]

Calculation	Operation							
	+	–	×	/	x^2	$\sqrt{x}$	sin x	$\|x\|$
I_{cxfq} (6)		1		1				
$V_{\mathrm{dcxf}} = \sqrt{6}\, V_{\mathrm{invxf}}$ with (4)	2	3	9	1		1	1	3
FFT I_{Lxn} *(complex)* [34]	13 566		4360					
I_{Lxn} [33]	7				14	7		
V_{dcxh} (12)	20	14	57	7	7	2	7	
V_{dcx} (2)	1				2	1		
Operations	13596	18	4426	9	23	11	8	3

Note: "+" addition, "–" subtraction, "×" multiplication, "/" division, "x^2" square, "$\sqrt{x}$" square root, "sin x" sine of an angle, "|x|" absolute.

TABLE II
REQUIRED NUMBER OF MATHEMATICAL OPERATORS FOR THE PROPOSED SIMPLIFIED MINIMUM V_{dcx} CALCULATION METHOD

Calculation	Operation							
	+	–	×	/	x^2	$\sqrt{x}$	sin x	$\|x\|$
$Q_{\mathrm{cx\_TCLCf}}(\alpha_x)$ (8)	2	2	7	2	1		1	
V_{dcxf} (7)		1	2	1		1		3
I_{Lxf} (14) (15)	1			2	2	1		
V_{dcxh} (13)			2			1		
V_{dcx} (2)	1				2	1		
Operations	4	3	11	5	5	4	1	3

Note: "+" addition, "–" subtraction, "×" multiplication, "/" division, "x^2" square, "$\sqrt{x}$" square root, "sin x" sine of an angle, "|x|" absolute.

TABLE III
SYSTEM AND TCLC-HAPF PARAMETERS

Parameters		Physical Values
System	f, v_{sx}, L_{sx}	*50 Hz, 110 V, 0.5 mH*
TCLC-HAPF	L_{c}, L_{PF}, C_{PF}, C_{dc}	*2.5 mH, 30 mH, 160 μF, 3300 μF*

C. Comparison Between Conventional and Proposed Minimum V_{dc} Calculation Methods

To compare the calculation steps between the conventional V_{dc} calculation method (based on FFT) [15], [16], [21] and the proposed V_{dc} calculation method for the TCLC-HAPF, Tables I and II summarize their required number of mathematical operators. The assumptions used in this comparison are 1) the considered harmonic current order is up to 23rd, and 2) the sampling rate is 25 kHz and 512-point FFT algorithms are used in the conventional method.

As shown in Table I, the conventional V_{dc} calculation method (based on the 512-point FFT algorithm [34]) requires a large amount of additions and multiplications. In contrast, the number of additions and multiplications used in the proposed method are 99.97% and 99.76% less than the conventional method as shown in Table II. Moreover, the other mathematical operators of the proposed method are also less than the conventional method by using FFT [15], [16], [21].

IV. CONTROL BLOCK OF THE PROPOSED ADAPTIVE DC-LINK VOLTAGE-CONTROLLED TCLC-HAPF

In this section, the control block of the adaptive dc-link voltage-controlled TCLC-HAPF is proposed based on the above-mentioned V_{dc} calculation method. And the overall control block diagram is shown in Fig. 5, which consists of the following three subcontrol blocks: 1) TCLC control block, 2) active VSI control block, and 3) adaptive dc-link voltage control block.

A. TCLC Control Block

For the TCLC control block as shown in Fig. 5, the fundamental load reactive power (Q_{Lxf}) is calculated by the single-phase instantaneous p–q theory [18], [25], which is used to control the firing angle (α_x) of the thyristor switch $(D_{1x}$ and $D_{2x})$. When Q_{Lxf} varies within the compensation range of the TCLC part, which means $Q_{\mathrm{cx\_TCLCf}}(\alpha_x = 180^o) < -Q_{\mathrm{Lxf}} < Q_{\mathrm{cx\_TCLCf}}(\alpha_x = 90^o)$, the corresponding α_x can be obtained from (8) with $Q_{\mathrm{cx\_TCLCf}}(\alpha_x) = -Q_{\mathrm{Lxf}}$. Otherwise, if Q_{Lxf} is outside the TCLC part compensation range, which means $Q_{\mathrm{cx\_TCLCf}}(\alpha_x = 180^o) > -Q_{\mathrm{Lxf}}$ or $Q_{\mathrm{cx\_TCLCf}}(\alpha_x = 90^o) < -Q_{\mathrm{Lxf}}$, α_x would be set to be equal to 180° or 90°, respectively. However, (8) has a term of $-2\alpha_x + \sin(2\alpha_x)$, which does not have a closed-form solution. Therefore, an LUT (Q_{Lxf} vs α_x) is built, so that α_x can be found according to the calculated Q_{Lxf} easily. Finally, the thyristor switches are triggered by comparing α_x to the phase angle of the load voltage (ϕ_{vx}), that is obtained from a phase lock loop. The TCLC part can compensate the reactive and unbalanced powers.

B. Active VSI Control Block

For the active VSI control part, the reference compensating reactive and harmonic current $(i_{\mathrm{cx_q}})$ is obtained through the three-phase instantaneous p–q theory [18], [35]. When the V_{dc} control is applied, $i_{\mathrm{cx_q}}$ is added with the dc-link voltage control feedback current signal $(i_{\mathrm{cx\_dc}})$, that is obtained from the V_{dc} control block, then it yields the final reference compensating current $(i_{\mathrm{cx}}*)$. Then, the compensating current error (Δi_{cx}), which defines as the difference between the sensed compensating current (i_{cx}) and $i_{\mathrm{cx}}*$, will be inputted to the hysteresis pulse width modulation (PWM) signal generator to generate the control trigger signals (T_{1x} and T_{2x}) of the VSI. The active VSI part can compensate the load harmonic current, improve the reactive power compensation ability and dynamic performance of the TCLC part, and also regulate the dc-link voltage to its reference value.

C. Adaptive DC-Link Voltage Control Block

The adaptive dc-link voltage control block contains the reference dc-link voltage calculation block and the dc-link voltage feedback control block.

1) Reference DC-Link Voltage Calculation Block: For the reference dc-link voltage calculation block, the simplified V_{dc} calculation method is used to calculate the phase required V_{dcx} value for the final reference dc-link voltage determination $(V_{\mathrm{dc}}*)$. All the input values such as α_x, Q_{Lxf}, $\bar{p}_{\mathrm{Lx}}$, and $\bar{q}_{\mathrm{Lx}}$ are obtained through the TCLC control block. Moreover, in

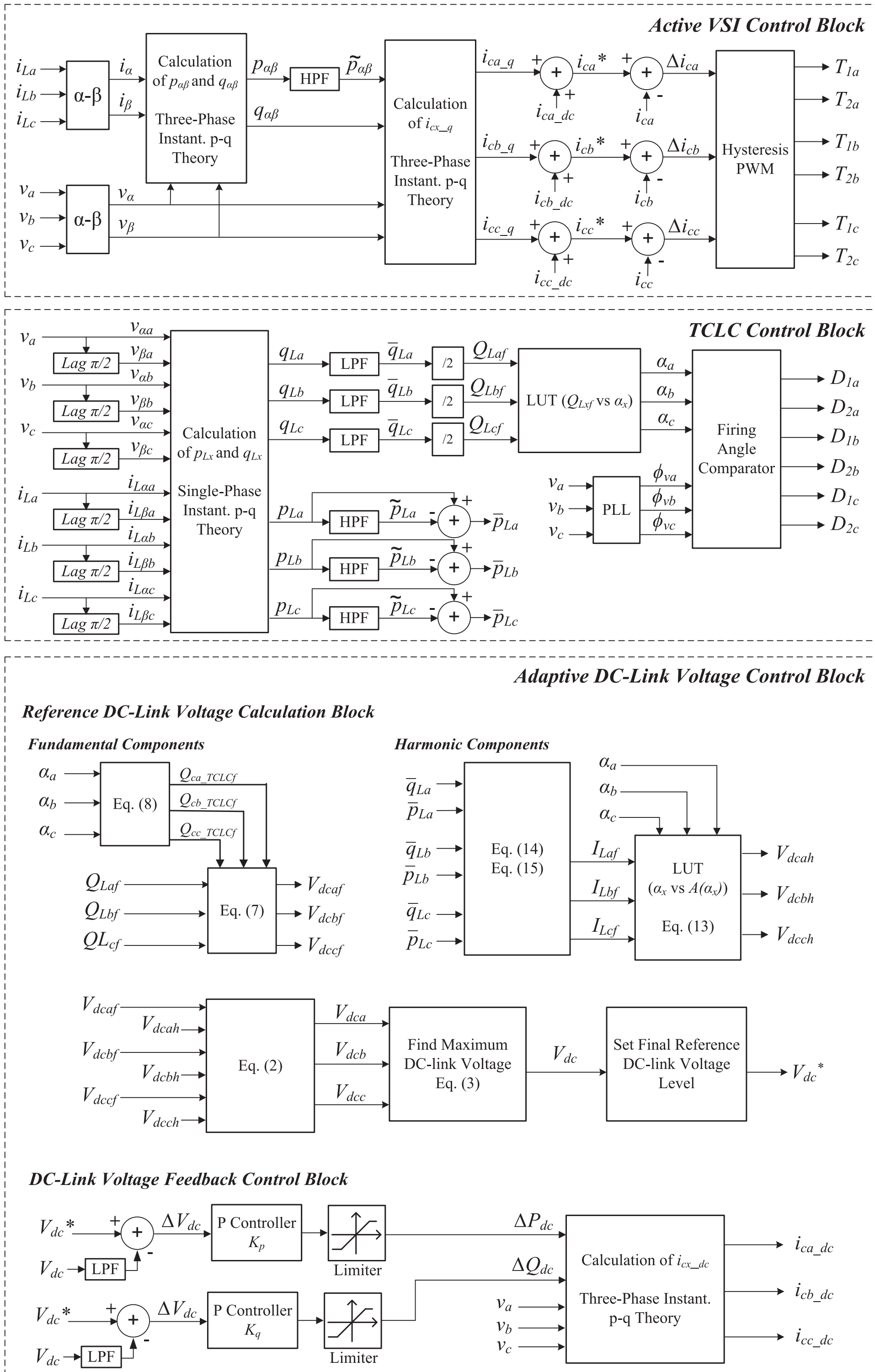

Fig. 5. Control block diagram of the adaptive dc-link voltage-controlled TCLC-HAPF.

order to stabilize $V_{\rm dc}$, $V_{\rm dc}*$ will be set to certain voltage levels range for selection [14].

2) DC-Link Voltage Feedback Control Block: For the dc-link voltage feedback control block, two proportional (P) controllers with the gains (K_p and K_q) are applied for generating the dc-link voltage feedback compensating current signals $i_{\rm cx\_dc}$ for the adaptive $V_{\rm dc}$ control. The dc-link voltage error signal ($\Delta V_{\rm dc}$), which is the difference between the reference $V_{\rm dc}*$ and the sensed $V_{\rm dc}$, would be input into two proportional controllers to generate the dc active and reactive feedback control signals ($\Delta P_{\rm dc}$ and $\Delta Q_{\rm dc}$) [13]. $\Delta Q_{\rm dc}$ is used to step change the dc-link voltage during the start-up process, while $\Delta P_{\rm dc}$ is used to maintain the dc-link voltage as its reference due to the system loss, in which the dc-link voltage control with feedback both active $\Delta P_{\rm dc}$ and reactive $\Delta Q_{\rm dc}$ components [13], [14], [16] can achieve both the start-up dc-link voltage self-charging function, maintaining the dc-link voltage and perform dynamic reactive power compensation simultaneously. Similar to the setting of the two controllers in [13], in order to simplify the control process, $\Delta P_{\rm dc}$ and $\Delta Q_{\rm dc}$ are actually calculated by the same controller, i.e., $K_p = K_q$ and $\Delta Q_{\rm dc} = -\Delta P_{\rm dc}$. Then, $\Delta P_{\rm dc}$ and $\Delta Q_{\rm dc}$ would be input to the three-phase instantaneous p–q theory [35] to generate the dc-link voltage feedback compensating current signal $(i_{\rm cx\_dc})$, which is used to update the reference $i_{\rm cx}*$ in the active VSI block in order to adaptively control the dc-link voltage of the TCLC-HAPF.

V. Simulation Case Studies

In this section, simulation case studies of the TCLC-HAPF compensation are executed by using the PSCAD/EMTDC platform. The parameters of the TCLC-HAPF system used in the simulations are summarized in Table III, and the maximum inductive and capacitive reactive power provided by the TCLC part is $Q_{\rm cx\_TCLCf}(\alpha_x = 90^o) = 647var$ and $Q_{\rm cx\_TCLCf}\ (\alpha_x = 180^o) = -633var$.

To verify the proposed $V_{\rm dc}$ calculation method and adaptive $V_{\rm dc}$ control for the TCLC-HAPF, two different balanced loading simulation case studies are performed, namely: 1) under the TCLC part reactive power compensation range and 2) over the TCLC part reactive power compensation range.

For under compensation case, the load varies from *Load* 1 to *Load* 2, the load reactive power changes from 70*var* to 103*var*, which is within the designed compensation range of the TCLC part of the TCLC-HAPF $(-633var < Q_{\rm cx\_TCLCf}\ (\alpha_x) < 647var)$. Moreover, the simulated TCLC-HAPF compensation performances with the proposed adaptive $V_{\rm dc}$ control will be compared with the conventional fixed $V_{\rm dc}$-controlled case.

For the over compensation case, when the *Load* 2 and *Load* 3 are connected to the system, the load reactive power rises to 936*var*, which is outside the TCLC part compensation range, the adaptive $V_{\rm dc}$ control can also help to increase the $V_{\rm dc}$ level to ensure the excessive load reactive power compensation.

In addition, with reference to the IEEE standard 519-2014 [36], the acceptable total demand distortion (TDD) ≤ 12% with $I_{\rm SC}/I_L$ is in 50 < 100 scale (a small rating 110 V–5 kVA simulation model and experimental prototype). The nominal-rated current is assumed to be equal to the fundamental load current at the worst case analysis, which results in THD = TDD ≤ 12%. Therefore, this paper evaluates the TCLC-HAPF current harmonics compensating performance by setting an acceptable THD ≤ 12%.

A. Under Compensation by Adaptive $V_{\rm dc}$-Controlled TCLC-HAPF

Fig. 6 shows the three-phase simulated system voltage and current before TCLC-HAPF compensation during *Load* 1 varying to *Load* 2. Table IV summarizes the corresponding simulation results before the TCLC-HAPF compensation. When *Load* 1 is connected, the three-phase simulated total harmonic distortion $(\mathrm{THD}i_{\rm sx})$ of the source current $(i_{\rm sx})$ is 27.9% and source power factor $(\mathrm{PF}_{\rm sx})$ is 0.96. When *Load* 2 is connected, $\mathrm{THD}i_{\rm sx}$ is 27.5% and $\mathrm{PF}_{\rm sx}$ is 0.96, in which both $\mathrm{THD}i_{\rm sx}$ cannot satisfy the IEEE Standard [36].

The calculated minimum $V_{\rm dc}$ values for compensating *Load* 1 and *Load* 2 by using the conventional FFT and the proposed methods are listed in Table V, where $V_{\rm dc}$ calculated by the proposed method can cover the $V_{\rm dc}$ value calculated by the conventional method, and the difference between them is small, which verifies the proposed minimum $V_{\rm dc}$ calculation method.

The three-phase simulated system voltage and current with the proposed adaptive $V_{\rm dc}$-controlled TCLC-HAPF compensation is shown in Figs. 7 and 8, and the corresponding compensation results are summarized in Table VI. Figs. 7 and 8 show the

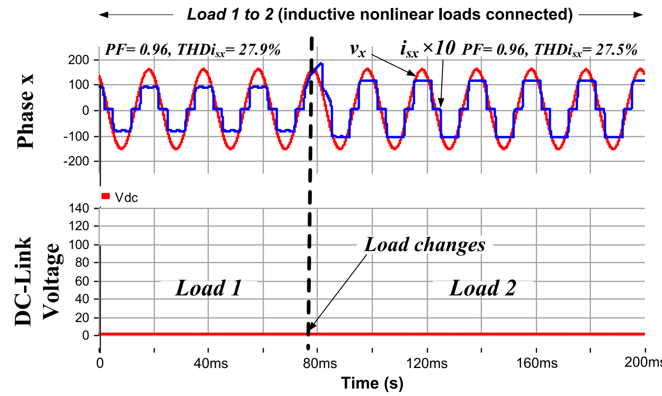

Fig. 6. Simulated system voltage and current before TCLC-HAPF compensation during under compensation case (*Load* 1 varying to *Load* 2).

TABLE IV
Simulation Results Before TCLC-HAPF Compensation During Under Compensation Case

Case:	Phase	$i_{\rm sx}$ $[A]$	$THDi_{\rm sx}$ $[\%]$	$Q_{\rm sxf}$ $[var]$	$PF_{\rm sx}$
Load 1	*a, b, c*	*6.69*	*27.9*	*70*	*0.96*
Load 2	*a, b, c*	*9.03*	*27.5*	*103*	*0.96*

TABLE V
Simulated Adaptive $V_{\rm dc}$ Levels of the TCLC-HAPF During Under Compensation Case

	Conventional Method with FFT	Proposed Method	Final Reference
Case:	Required $V_{\rm dc}$	Required $V_{\rm dc}$	$V_{\rm dc}$ Level
Load 1	*24.8 V*	*26.1 V*	*30 V*
Load 2	*32.2 V*	*33.7 V*	*40 V*

TABLE VI
Simulation Results After Adaptive $V_{\rm dc}$-Controlled TCLC-HAPF Compensation During Under Compensation Case

Case:	Phase	$i_{\rm sx}$ $[A]$	$THDi_{\rm sx}$ $[\%]$	$Q_{\rm sxf}$ $[var]$	$PF_{\rm sx}$
Load 1	*a, b, c*	*6.71*	*8.0*	*11*	*0.99*
Load 2	*a, b, c*	*8.73*	*8.3*	*11*	*0.99*

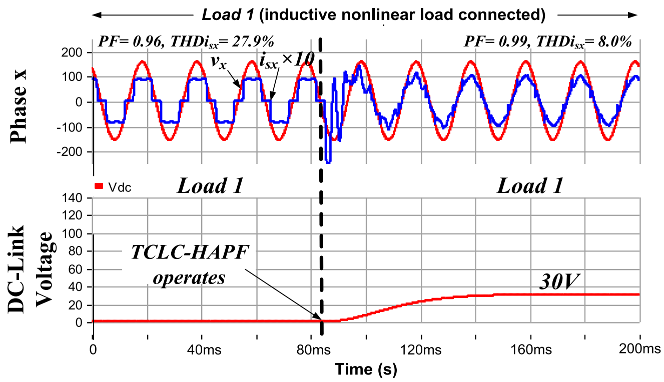

Fig. 7. Simulated system voltage and current with the adaptive $V_{\rm dc}$-controlled TCLC-HAPF compensation during starts operation at *Load* 1.

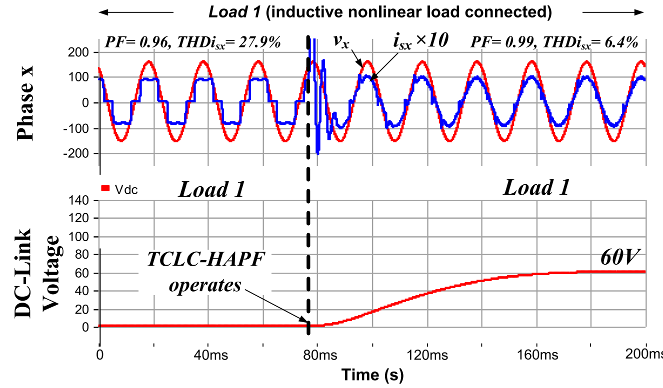

Fig. 9. Simulated system voltage and current with the fixed $V_{\rm dc}$-controlled TCLC-HAPF compensation during starts operation at *Load* 1.

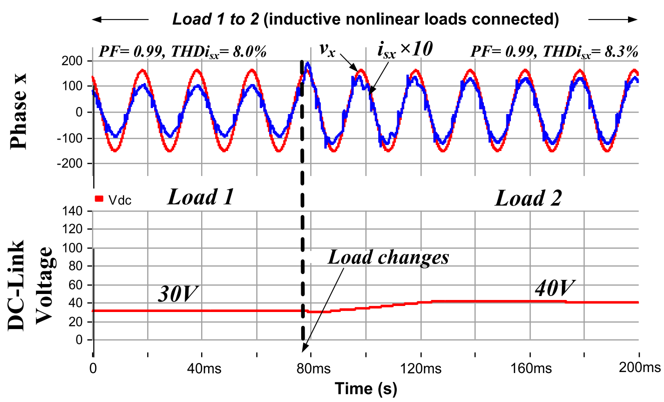

Fig. 8. Simulated system voltage and current with the adaptive $V_{\rm dc}$-controlled TCLC-HAPF compensation during under compensation case (*Load* 1 varying to *Load* 2).

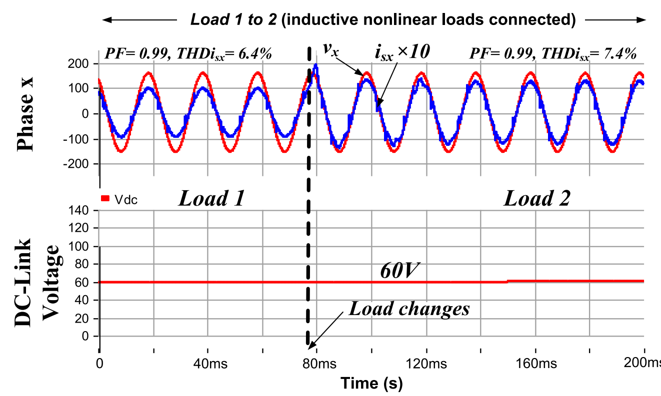

Fig. 10. Simulated system voltage and current with the fixed $V_{\rm dc}$-controlled TCLC-HAPF compensation during under compensation case (*Load* 1 varying to *Load* 2).

TABLE VII
SIMULATION RESULTS AFTER FIXED $V_{\rm dc} = 60$ V-CONTROLLED TCLC-HAPF COMPENSATION DURING UNDER COMPENSATION CASE

Case:	Phase	$I_{\rm sx}$ $[A]$	$THDi_{\rm sx}$ $[\%]$	$Q_{\rm sxf}$ $[var]$	$PF_{\rm sx}$
Load 1	*a, b, c*	*6.76*	*6.4*	*20*	*0.99*
Load 2	*a, b, c*	*8.77*	*7.4*	*26*	*0.99*

adaptive $V_{\rm dc}$-controlled TCLC-HAPF during starts operation at *Load* 1, and during *Load* 1 varying to *Load* 2. From Figs. 7 and 8, they show that $V_{\rm dc}$ level is changing adaptively according to the load variations. Table VI shows that $\text{THD}i_{\rm sx}$ decreases to less than 9% and $\text{PF}_{\rm sx}$ is improved to 0.99 after the adaptive $V_{\rm dc}$-controlled TCLC-HAPF compensation, in which $\text{THD}i_{\rm sx}$ satisfy the IEEE Standard [36].

To compare with the adaptive $V_{\rm dc}$ control method, a fixed $V_{\rm dc} = 60$ V control is applied to the TCLC-HAPF. Figs. 9 and 10 show the fixed $V_{\rm dc}$-controlled TCLC-HAPF during starts operation at *Load* 1, and during *Load* 1 varying to *Load* 2. Table VII summarizes the corresponding compensation results. The compensated $\text{THD}i_{\rm sx}$ decreases to less than 8% and $\text{PF}_{\rm sx}$ is improved to 0.99 after the fixed $V_{\rm dc}$-controlled TCLC-HAPF compensation. Comparing Fig. 10 with Fig. 8, the fixed and adaptive dc voltage control can obtain similar steady-state compensation results. But the proposed control strategy solely requires lower dc voltage levels for compensation. Moreover, Fig. 11 shows the compensating current $i_{\rm ca}$ of phase *a* and its frequency spectrum with THD values for the fixed and proposed adaptive $V_{\rm dc}$-controlled TCLC-HAPF. From Fig. 11, $i_{\rm ca}$ of the adaptive $V_{\rm dc}$ control method obtains lower switching noise than the fixed $V_{\rm dc}$ case.

Based on the above simulation results, they show that the TCLC part can compensate the load reactive power, and $V_{\rm dc}$ provided by the VSI of the TCLC-HAPF can deal with the harmonic current problem. Figs. 6–11, verify 1) the proposed minimum $V_{\rm dc}$ calculation method and 2) the adaptive $V_{\rm dc}$-controlled TCLC-HAPF can adaptively change $V_{\rm dc}$ to obtain lower switching noise and similar compensation performances compared with the fixed $V_{\rm dc}$ case.

B. Over Compensation by Adaptive $V_{\rm dc}$-Controlled TCLC-HAPF

Fig. 12 shows the three-phase simulated system voltage and current before TCLC-HAPF compensation during *Load* 2 varying to *Load* 2+*Load* 3. Table VIII summarizes the corresponding simulation results for *Load* 2+*Load* 3 before the TCLC-HAPF compensation. When *Load* 2+*Load* 3 are connected to the system, the three-phase simulated $\text{THD}i_{\rm sx}$ becomes 16.4% and

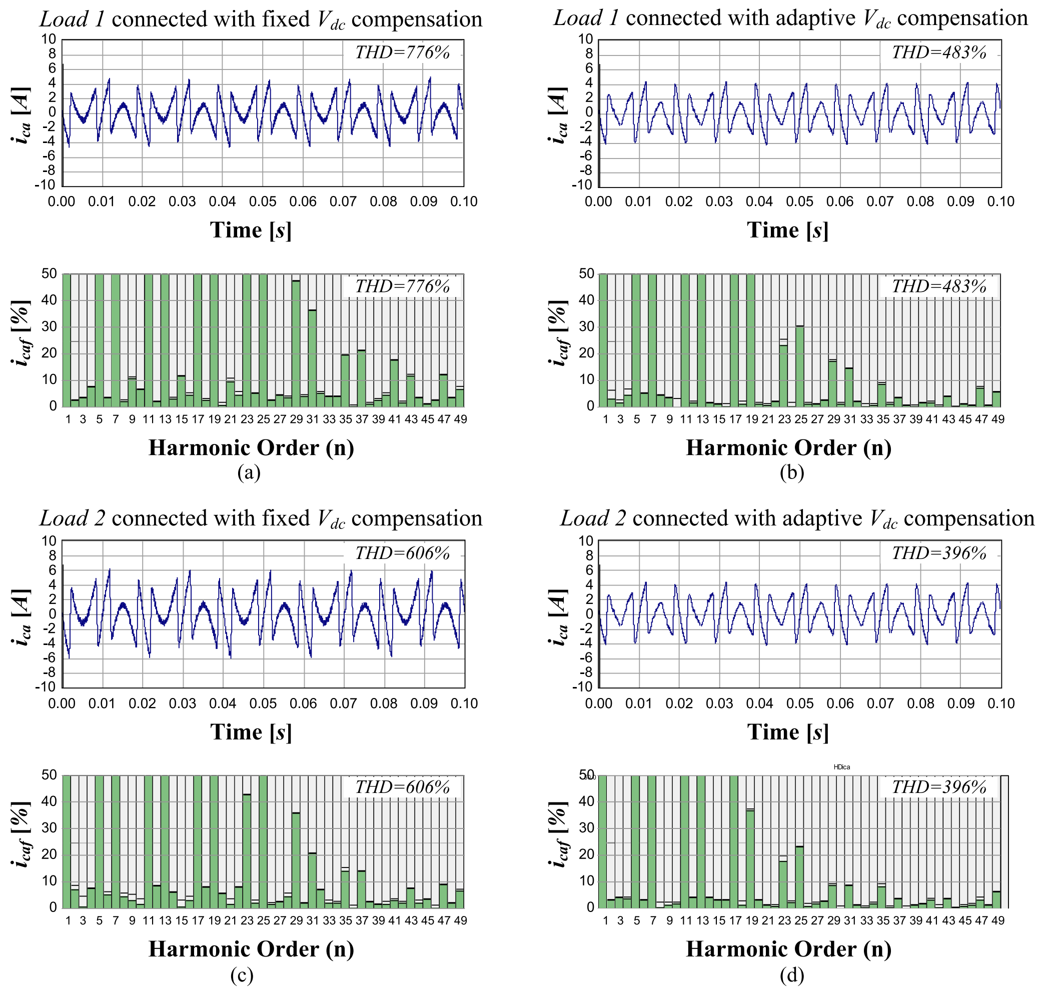

Fig. 11. Simulated i_{ca} and its frequency spectrum with (a) fixed V_{dc} for *Load* 1, (b) adaptive V_{dc} control for *Load* 1, (c) fixed V_{dc} for *Load* 2, and (d) adaptive V_{dc} control for *Load* 2.

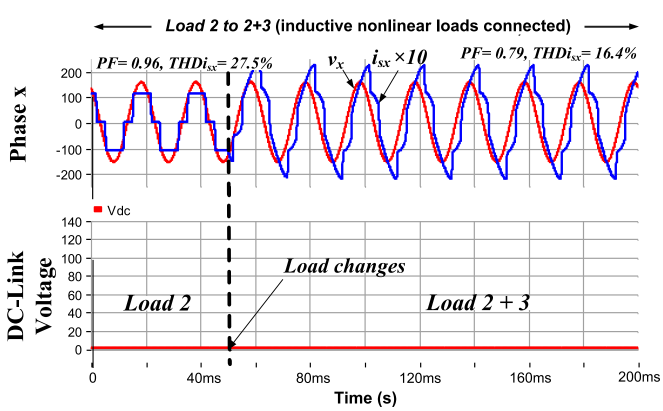

Fig. 12. Simulated system voltage and current before TCLC-HAPF compensation during over compensation case (*Load* 2 varying to *Load* 2+3).

TABLE VIII
SIMULATION RESULTS BEFORE TCLC-HAPF COMPENSATION DURING OVER COMPENSATION CASE

Case:	Phase	I_{sx} $[A]$	$THDi_{\mathrm{sx}}$ $[\%]$	Q_{sxf} $[var]$	PF_{sx}
Load 2 + Load 3	*a, b, c*	*14.4*	*16.4*	*936*	*0.79*

TABLE IX
SIMULATED ADAPTIVE V_{dc} LEVEL OF THE TCLC-HAPF DURING OVER COMPENSATION CASE

Case:	Required V_{dc}	V_{dc} Level
Load 2 + Load 3	*119.5 V*	*120 V*

$\mathrm{PF_{sx}}$ becomes 0.79, in which $\mathrm{THD}i_{\mathrm{sx}}$ cannot satisfy the IEEE Standard [36].

The calculated required minimum V_{dc} values for compensating *Load* 2+*Load* 3 case are listed in Table IX. Fig. 13 shows the three-phase simulated system voltage and current with the proposed adaptive V_{dc}-controlled TCLC-HAPF compensation and Table X summarizes the corresponding compensation results. When *Load* 2+*Load* 3 are connected to the system, the V_{dc} level adaptively changes from 40 to 120 V according to the load condition, the $\mathrm{THD}i_{\mathrm{sx}}$ and $\mathrm{PF_{sx}}$ are compensated to 4.0% and 0.99, respectively.

According to the simulation results of the over compensation case, when the TCLC part of the TCLC-HAPF cannot provide sufficient reactive power to the loads, the proposed adaptive V_{dc}

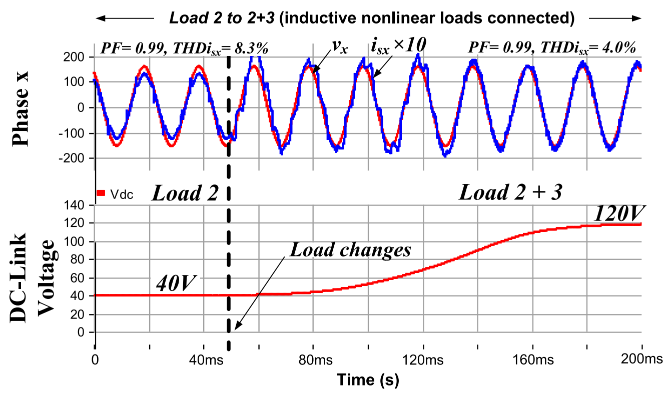

Fig. 13. Simulated system voltage and current with the adaptive V_{dc}-controlled TCLC-HAPF compensation during over compensation case (*Load* 2 varying to *Load* 2+3).

TABLE X
SIMULATION RESULTS AFTER ADAPTIVE V_{dc}-CONTROLLED TCLC-HAPF COMPENSATION DURING OVER COMPENSATION CASE

Case:	Phase	I_{sx} $[A]$	$THDi_{\mathrm{sx}}$ $[\%]$	Q_{sxf} $[var]$	PF_{sx}
Load 2 + Load 3	*a, b, c*	*11.8*	*4.0*	*89*	*0.99*

control method can also dynamically increase the V_{dc} level to increase the TCLC-HAPF reactive power compensation range.

Figs. 12 and 13, and Tables VIII–X verify that the adaptive V_{dc}-controlled TCLC-HAPF can dynamically compensate the reactive power and suppress the current harmonics when the load reactive power falls outside the TCLC part compensation range.

VI. EXPERIMENTAL RESULTS

The following experimental results are performed on an 110 V-5 kVA three-phase three-wire TCLC-HAPF laboratory prototype. The control system of the TCLC-HAPF is composed of two paralleled DSP-TMS320F2812s to separately control the TCLC part and the active inverter part. For the TCLC part, the thyristor modules are SanRex PK110FG160. For the active inverter part, the insulated gate bipolar transistors are PM300DSA60. The system and the TCLC-HAPF parameters as shown in Table III are also used for the experimental testing. However, owing to the current limitation of the laboratory prototype, only under compensation case will be tested in this section. The adaptive dc-link voltage-controlled TCLC-HAPF is verified in the following two parts: 1) the dynamic performance of the TCLC-HAPF according to the load variation (*Load* 1 varies to *Load* 2); 2) the comparison of the VSI switching noise and switching loss with the fixed V_{dc}-controlled TCLC-HAPF.

Fig. 14 shows the three-phase experimental system voltage and current before the TCLC-HAPF compensation during *Load* 1 varying to *Load* 2, and Table XI lists the experimental results before the TCLC-HAPF compensation. When *Load* 1 is connected, the three-phase $\mathrm{THD}i_{\mathrm{sx}}$ values are 24.5%, 23.7%, and 24.1%, and $\mathrm{PF}_{\mathrm{sx}}$ values are 0.96, 0.96, and 0.96, respectively. When *Load* 2 is connected, the three-phase $\mathrm{THD}i_{\mathrm{sx}}$ are

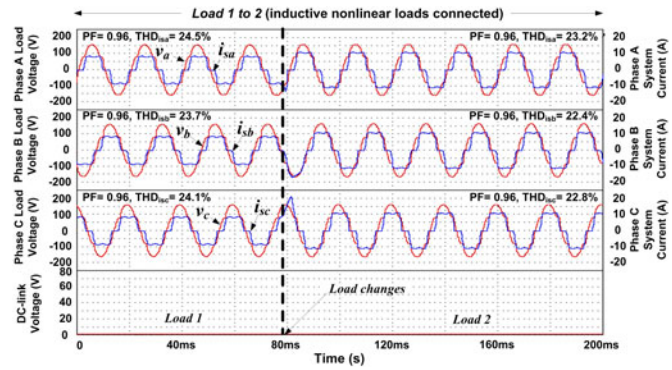

Fig. 14. Three-phase experimental system voltage and current before the TCLC-HAPF compensation during *Load* 1 varying to *Load* 2.

TABLE XI
EXPERIMENTAL RESULTS BEFORE TCLC-HAPF COMPENSATION DURING *LOAD 1* TO *LOAD 2*

Case:	Phase	i_{sx} $[A]$	$THDi_{\mathrm{sx}}$ $[\%]$	Q_{sxf} $[var]$	PF_{sx}
Load 1	*a*	*6.6*	*24.5*	*80*	*0.96*
	b	*6.7*	*23.7*	*80*	*0.96*
	c	*6.6*	*24.1*	*80*	*0.96*
Load 2	*a*	*8.7*	*23.2*	*110*	*0.96*
	b	*8.5*	*22.4*	*110*	*0.96*
	c	*8.5*	*22.8*	*110*	*0.96*

TABLE XII
EXPERIMENTAL ADAPTIVE V_{dc} LEVELS OF THE TCLC-HAPF DURING *LOAD 1* AND *LOAD 2* CASES

Case:	Required V_{dc}	V_{dc} Level
Load 1	*25.1 V*	*30 V*
Load 2	*35.1 V*	*40 V*

23.2%, 22.4%, 22.8% and $\mathrm{PF}_{\mathrm{sx}}$ values are 0.96, 0.96, 0.96, respectively, in which the $\mathrm{THD}i_{\mathrm{sx}}$ for both loadings cannot satisfy the IEEE Standard [36].

According to the proposed simplified minimum V_{dc} calculation method, the required V_{dc} of the adaptive V_{dc}-controlled TCLC-HAPF compensation for *Load* 1 and *Load* 2 are listed in Table XII.

A. Dynamic Performance of Adaptive V_{dc}-Controlled TCLC-HAPF to Load Variation

Figs. 15 and 16 show the three-phase experimental system voltage and current with the adaptive V_{dc}-controlled TCLC-HAPF during starts operation at *Load* 1, and during *Load* 1 varying to *Load* 2. The corresponding experimental results after the adaptive V_{dc}-controlled TCLC-HAPF compensation are summarized in Table XIII.

When *Load* 1 is connected, the V_{dc} level rises to 30 V, the compensated $\mathrm{THD}i_{\mathrm{sx}}$ values become 7.9%, 7.2%, 7.5%. When *Load* 2 is connected, the V_{dc} level adaptively changes to 40 V, the $\mathrm{THD}i_{\mathrm{sx}}$ values become 6.8%, 5.8%, 6.4%, in which the $\mathrm{THD}i_{\mathrm{sx}}$ values for both loadings satisfy the IEEE Standard [36]. And the three-phase $\mathrm{PF}_{\mathrm{sx}}$ values for both *Load* 1 and

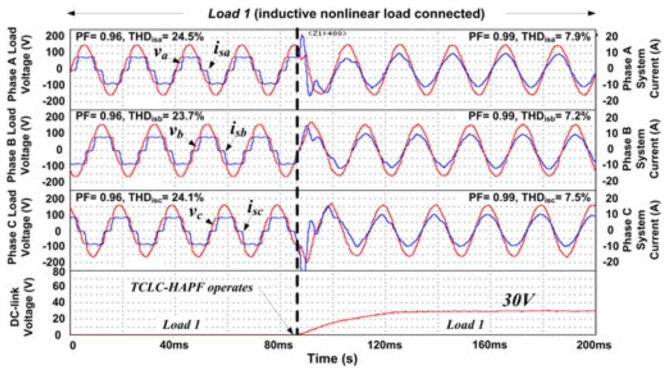

Fig. 15. Three-phase experimental system voltage and current with the adaptive V_{dc}-controlled TCLC-HAPF compensation during starts operation at *Load* 1.

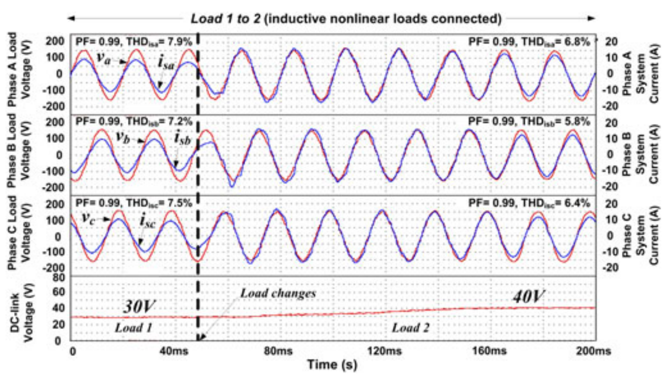

Fig. 16. Three-phase experimental system voltage and current with the adaptive V_{dc}-controlled TCLC-HAPF compensation during *Load* 1 varying to *Load* 2.

TABLE XIII
EXPERIMENTAL RESULTS AFTER THE ADAPTIVE V_{dc}-CONTROLLED TCLC-HAPF COMPENSATION DURING *LOAD 1* TO *LOAD 2*

Case:	Phase	$I_{\mathrm{sx}}\ [A]$	$THD\mathrm{i}_{\mathrm{sx}}\ [\%]$	$Q_{\mathrm{sxf}}\ [var]$	PF_{sx}
Load 1	*a*	*6.8*	*7.9*	*20*	*0.99*
	b	*6.8*	*7.2*	*10*	*0.99*
	c	*6.8*	*7.5*	*10*	*0.99*
Load 2	*a*	*8.8*	*6.8*	*20*	*0.99*
	b	*8.7*	*5.8*	*20*	*0.99*
	c	*8.8*	*6.4*	*30*	*0.99*

Load 2 cases are improved to 0.99 after compensation. Figs. 15 and 16 and Tables XI and XIII verify the adaptive V_{dc} control method for TCLC-HAPF reactive power and current harmonics compensation.

B. Comparison With Fixed V_{dc}-Controlled TCLC-HAPF

To compare with the adaptive V_{dc} control method, a fixed $V_{\mathrm{dc}} = 60\,\mathrm{V}$ control is applied to the TCLC-HAPF. Figs. 17 and 18 show the three-phase experimental system voltage and current with the fixed V_{dc}-controlled TCLC-HAPF during starts operation at *Load* 1, and during *Load* 1 varying to *Load* 2 and Table XIV summarizes the corresponding experimental compensation results. From Table XIV, it shows the three-phase

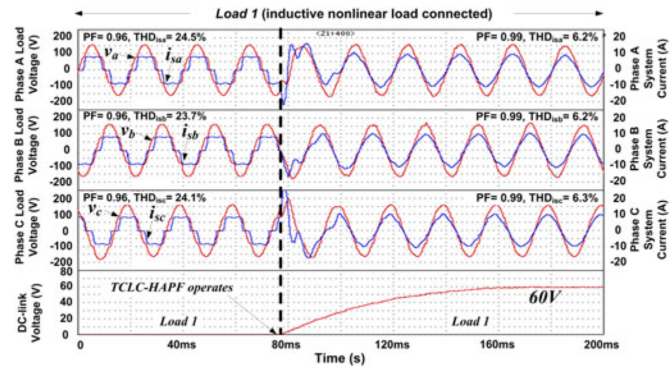

Fig. 17. Three-phase experimental system voltage and current with the fixed V_{dc}-controlled TCLC-HAPF compensation during starts operation at *Load* 1.

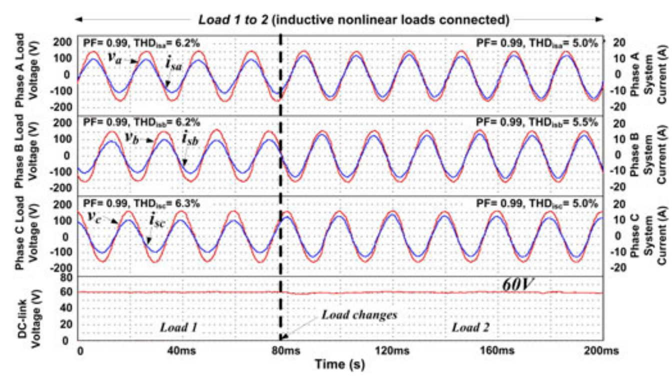

Fig. 18. Three-phase experimental system voltage and current with the fixed V_{dc}-controlled TCLC-HAPF compensation during *Load* 1 varying to *Load* 2.

TABLE XIV
EXPERIMENTAL RESULTS AFTER FIXED V_{dc}-CONTROLLED TCLC-HAPF COMPENSATION DURING *LOAD 1* TO *LOAD 2*

Case:	Phase	$I_{\mathrm{sx}}\ [A]$	$THDi_{\mathrm{sx}}\ [\%]$	$Q_{\mathrm{sxf}}\ [var]$	PF_{sx}
Load 1	*a*	*7.0*	*6.2*	*10*	*0.99*
	b	*7.0*	*6.2*	*10*	*0.99*
	c	*6.9*	*6.3*	*20*	*0.99*
Load 2	*a*	*9.0*	*5.0*	*20*	*0.99*
	b	*8.9*	*5.5*	*10*	*0.99*
	c	*9.0*	*5.0*	*20*	*0.99*

$\mathrm{THD}i_{\mathrm{sx}}$ values have been reduced to 6.2%, 6.2%, 6.3% for *Load* 1, and 5.0%, 5.5%, 5.0% for *Load* 2; and $\mathrm{PF}_{\mathrm{sx}}$ is compensated to above 0.99 after compensation, in which the $\mathrm{THD}i_{\mathrm{sx}}$ values for both loadings satisfy the IEEE Standard [36].

Moreover, Fig. 19 shows the compensating current i_{ca} of phase *a* and its frequency spectrum with THD value for the fixed and proposed adaptive V_{dc}-controlled TCLC-HAPF. From Fig. 19, i_{ca} of the adaptive V_{dc}-controlled TCLC-HAPF obtains lower switching noise than the fixed V_{dc} case.

Furthermore, referred to the VSI power loss calculation method in [37], the experimental switching loss results for compensating *Load* 1 and *Load* 2 by the fixed and adaptive V_{dc}-controlled TCLC-HAPF are shown in Table XV. From Table XV, the switching power loss can be reduced by 17% and 18% for *Load* 1 and *Load* 2 by the adaptive V_{dc}

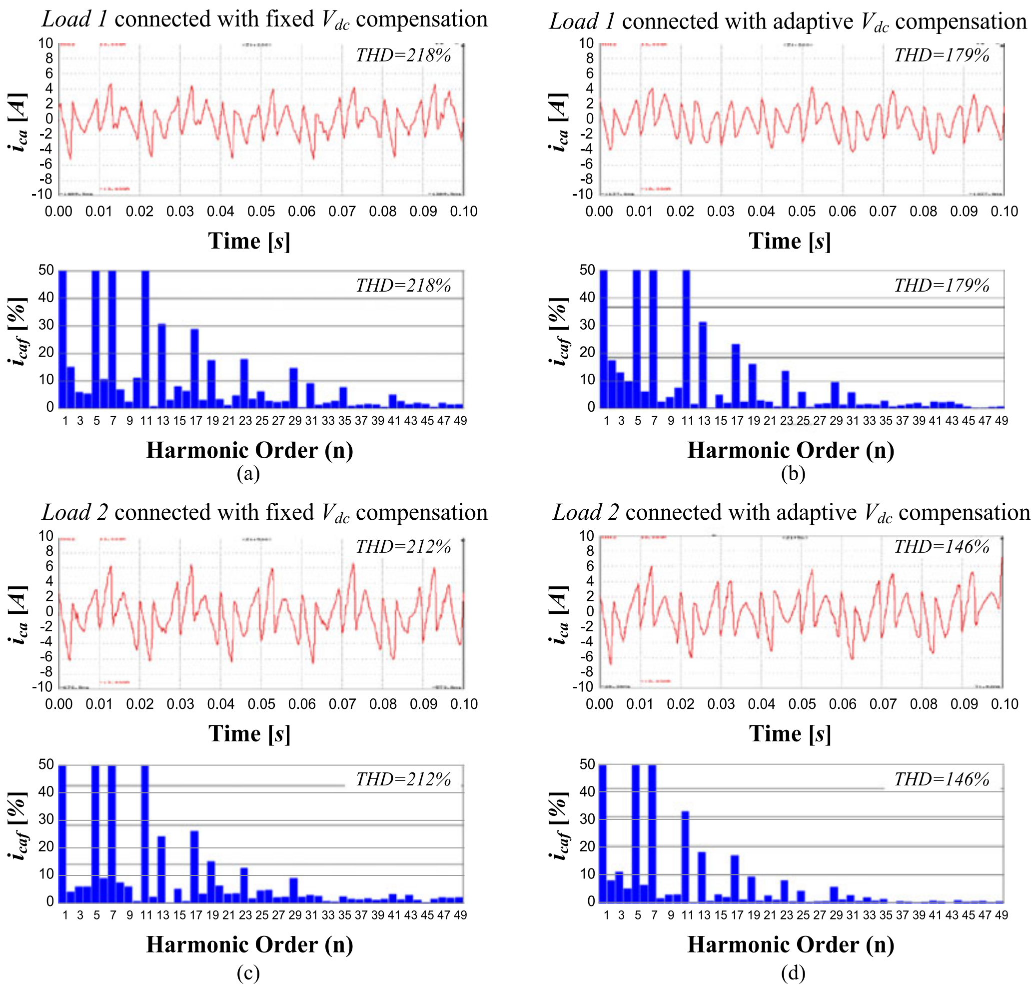

Fig. 19. Experimental i_{ca} and its frequency spectrum with (a) fixed $V_{\mathrm{dc}} = 60\ \mathrm{V}$ for *Load* 1, (b) adaptive V_{dc} control for *Load* 1, (c) fixed $V_{\mathrm{dc}} = 60\mathrm{V}$ for *Load* 2, and (d) adaptive V_{dc} control for *Load* 2.

TABLE XV
EXPERIMENTAL VSI POWER LOSS BETWEEN FIXED AND ADAPTIVE V_{dc}-CONTROLLED TCLC-HAPF DURING *LOAD 1* TO *LOAD 2*

	Power Loss [*W*]	
Case:	Fixed $V_{\mathrm{dc}} = 60V$	Adaptive V_{dc}
Load 1	*141 W*	*117 W* ($V_{\mathrm{dc}} = 30$ V), ↓*17%*
Load 2	*147 W*	*120 W* ($V_{\mathrm{dc}} = 40$ V), ↓*18%*

control. Therefore, Fig. 19 and Table XV verify that the adaptive V_{dc} control method for TCLC-HAPF can reduce the switching noise and switching loss and obtain similar steady-state compensation results in comparison with the fixed V_{dc} control method.

For the proposed control strategy, due to its final reference V_{dc}^* is varying at different loading cases, the compensating performance is affected at each V_{dc} varying. Compared with the fixed V_{dc} one, the adaptive one obtains a longer settling time during both the loading and V_{dc} level varying case. Moreover, its dynamic response will be sacrificed a little bit under an adaptive low dc operating voltage.

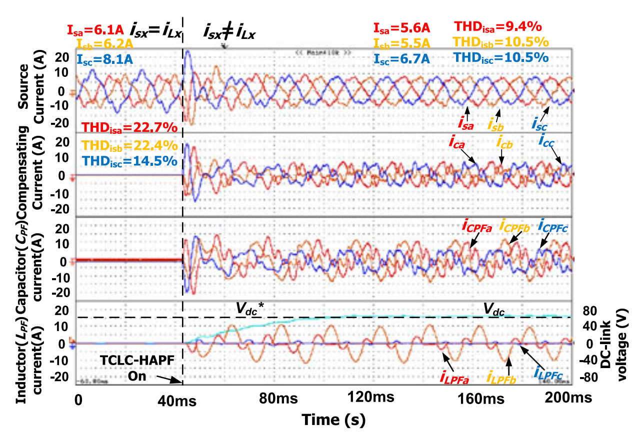

Fig. 20. Experimental results of dynamic performance by using the proposed adaptive V_{dc}-controlled TCLC-HAPF during unbalanced loading compensation: source currents, compensating currents, capacitor (C_{PF}) currents, inductor (L_{PF}) currents and dc-link voltage.

C. Proposed Adaptive DC-Link Voltage-Controlled TCLC-HAPF for Unbalanced Loading Compensation

Fig. 20 shows the experimental results of dynamic performance by using the proposed adaptive V_{dc}–controlled

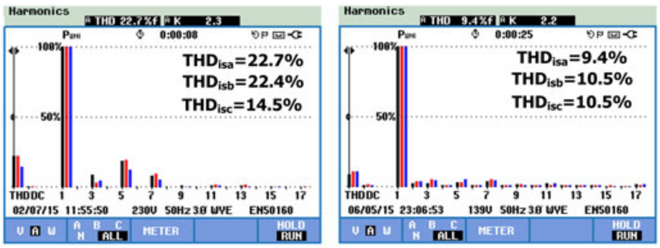

(a) (b)

Fig. 21. Experimental system current spectrums (a) before compensation, (b) after the proposed adaptive $V_{\rm dc}$-controlled TCLC-HAPF compensation.

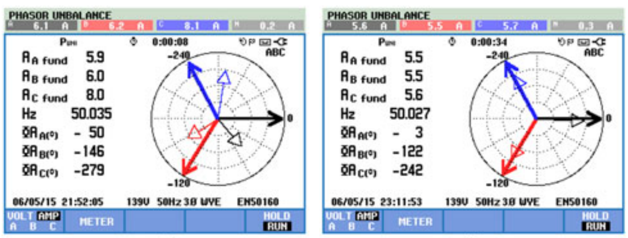

(a) (b)

Fig. 22. Experimental phasor diagrams of system voltages and currents (a) before compensation, and (b) after the proposed adaptive $V_{\rm dc}$-controlled TCLC-HAPF compensation.

TCLC-HAPF during unbalanced loading compensation. Figs. 21 and 22 show the experimental system current spectrums and phasor diagrams of the system voltages and currents before and after the adaptive $V_{\rm dc}$–controlled TCLC-HAPF compensation. From Figs. 21 and 22, the experimental $\text{THD}i_{\rm sx}$ have been compensated to 10.5% (showing the worst phase), in which the compensated $\text{THD}i_{\rm sx}$ satisfy the IEEE Standard [36]. And the compensated system voltage and current are in phase for all the three phases, and the three-phase experimental system currents become approximately balanced after TCLC-HAPF compensation. Figs. 20–22 prove that the proposed adaptive $V_{\rm dc}$ control method for the TCLC-HAPF can work well under unbalanced loading compensation.

VII. Conclusion

In this paper, the adaptive dc-link voltage controller for the three-phase three-wire TCLC-HAPF is proposed. Different from the conventional $V_{\rm dc}$ calculation method based on the complicated FFT, the proposed $V_{\rm dc}$ calculation can significantly reduce a large number of calculation steps, thus simplifying the $V_{\rm dc}$ calculation. On the other hand, the proposed adaptive dc-link voltage control method for TCLC-HAPF can achieve satisfactory compensation performance, low switching loss, and switching noise simultaneously. Finally, simulation and experimental results verify both adaptive dc-link voltage controller for the TCLC-HAPF and the proposed simplified $V_{\rm dc}$ calculation method.

References

[1] Q. Xu, F. Ma, A. Luo, Z. He, and H. Xiao, "Analysis and control of M3C based UPQC for power quality improvement in medium/high voltage power grid," *IEEE Trans. Power Electron.*, vol. 31, no. 12, pp. 8182–8194, Dec. 2016, doi: 10.1109/TPEL.2016.2520586

[2] W. R. N. Santos, E. D. M. Fernandes, E. R. C. D. Silva, C. B. Jacobina, A. C. Oliveira, and P. M. Santos, "Transformerless single-phase universal active filter with UPS features and reduced number of electronic power switches," *IEEE Trans. Power Electron.*, vol. 31, no. 6, pp. 4111–4120, Jun. 2016.

[3] W. R. N. Santos *et al.*, "The transformerless single-phase universal active power filter for harmonic and reactive power compensation," *IEEE Trans. Power Electron.*, vol. 29, no. 7, pp. 3563–3572, Jul. 2014.

[4] M. C. Wong *et al.*, "Self-reconfiguration property of a mixed signal controller for improving power quality compensation during light loading," *IEEE Trans. Power Electron.*, vol. 30, no. 10, pp. 5938–5951, Oct. 2015.

[5] L. Limongi, L. D. S. Filho, L. Genu, F. Bradaschia, and M. Cavalcanti, "Transformerless hybrid power filter based on a six-switch two-leg inverter for improved harmonic compensation performance," *IEEE Trans. Ind. Electron.*, vol. 62, no. 1, pp. 40–51, Jan. 2015.

[6] C. Kumar and M. K. Mishra, "An improved hybrid DSTATCOM topology to compensate reactive and nonlinear loads," *IEEE Trans. Ind. Electron.*, vol. 61, no. 12, pp. 6517–6527, Dec. 2014.

[7] B. Singh, K. Al-Haddad, and A. Chandra, "A review of active filters for power quality improvement," *IEEE Trans. Ind. Electron.*, vol. 45, no. 5, pp. 960–971, Oct. 1999.

[8] F. Z. Peng, H. Akagi, and A. Nabae, "A new approach to harmonic compensation in power systems—A combined system of shunt passive and series active filters," *IEEE Trans. Ind. Appl.*, vol. 26, no. 6, pp. 983–990, Nov./Dec.1990.

[9] S. P. Litrán and P. Salmerón, "Reference voltage optimization of a hybrid filter for nonlinear load compensation," *IEEE Trans. Ind. Electron.*, vol. 61, no. 6, pp. 2648–2654, Jun. 2014.

[10] J. C. A.-Gil, E. Pérez, C. Ariño, and H. Beltran, "Optimization algorithm for selective compensation in a shunt active power filter," *IEEE Trans. Ind. Electron.*, vol. 62, no. 6, pp. 3351–3361, Jun. 2015.

[11] E. S. Sreeraj, E. K. Prejith, K. Chatterjee, and S. Bandyopadhyay, "An active harmonic filter based on one-cycle control," *IEEE Trans. Ind. Electron.*, vol. 61, no. 8, pp. 3799–3809, Jun. 2015.

[12] S. Srianthumrong and H. Akagi, "A medium-voltage transformerless ac/dc power conversion system consisting of a diode rectifier and a shunt hybrid filter," *IEEE Trans. Ind. Appl.*, vol. 39, no. 3, pp. 874–882, May 2003.

[13] W. H. Choi, C. S. Lam, M. C. Wong, and Y. D. Han, "Analysis of dc-link voltage controls in three-phase four-wire hybrid active power filters," *IEEE Trans. Power Electron.*, vol. 28, no. 5, pp. 2180–2191, May 2013.

[14] C. S. Lam, W. H. Choi, M. C. Wong, and Y. D. Han, "Adaptive dc-link voltage controlled hybrid active power filters for reactive power compensation," *IEEE Trans. Power Electron.*, vol. 27, no. 4, pp. 1758–1772, Apr. 2012.

[15] C. S. Lam, X. X. Cui, W. H. Choi, M. C. Wong, and Y. D. Han, "Minimum inverter capacity design for three-phase four-wire LC-hybrid active power filters," *IET Power Electron.*, vol. 5, no. 7, pp. 956–968, Aug. 2012.

[16] C. S. Lam, M. C. Wong, W.-H. Choi, X.-X. Cui, H.-M. Mei, and J.-Z. Liu, "Design and performance of an adaptive low-dc-voltage-controlled LC-hybrid active power filter with a neutral inductor in three-phase four-wire power systems," *IEEE Trans. Ind. Electron.*, vol. 61, no. 6, pp. 2635–2647, Jun. 2014.

[17] S. Rahmani, A. Hamadi, and K. Al-Haddad, "A combination of shunt hybrid power filter and thyristor-controlled reactor for power quality," *IEEE Trans. Ind. Electron.*, vol. 61, no. 5, pp. 2152–2164, May 2014.

[18] L. Wang, C. S. Lam, and M. C. Wong, "An unbalanced control strategy for a thyristor controlled LC-coupling hybrid active power filter (TCLC-HAPF) in three-phase three-wire systems," *IEEE Trans. Power Electron.*, vol. 32, no. 2, pp. 1056–1069, Feb. 2017.

[19] L. Wang, C. S. Lam, and M. C. Wong, "A hybrid-STATCOM with wide compensation range and low dc-link voltage," *IEEE Trans. Ind. Electron.*, vol. 63, no. 6, pp. 3333–3343, Jun. 2016.

[20] M. C. Wong, J. Tang, and Y.-D. Han, "Cylindrical coordinate control of three-dimensional PWM technique in three-phase four-wired trilevel inverter," *IEEE Trans. Power Electron.*, vol. 18, no. 1, pp. 208–220, Jan. 2003.

[21] C. S. Lam, X. X. Cui, M. C. Wong, and Y. D. Han, "Minimum dc-link voltage design of three-phase four-wire active power filters," in *Proc. 2012 IEEE 13th Workshop Control Model. Power Electron.*, Jun. 2012, pp. 1–5.

[22] A. M. Al-Zamil and D. A. Torrey, "A passive series, active shunt filter for high power applications," *IEEE Trans. Power Electron.*, vol. 16, no. 1, pp. 101–109, Jan. 2001.

[23] G. K. Singh, A. K. Singh, and R. Mitra, "A simple fuzzy logic based robust active power filter for harmonics minimization under random load variation," *Electr. Power Syst. Res.*, vol. 77, no. 8, pp. 1101–1111, Jun. 2007.

[24] M. A. Ahmed, S. A. Zaid, and O. A. Mahgoub, “A simplified control strategy for the shunt active power filter for harmonic and reactive power compensation,” *J. Electr. Eng.*, vol. 11, pp. 1–7, 2011.

[25] V. Khadkikar, A. Chandra, and B. N. Singh, “Generalized single-phase p–q theory for active power filtering: Simulation and DSP-based experimental investigation,” *IET Power Electron.*, vol. 2, pp. 67–78, Jan. 2009.

[26] J. Lundquist, “On harmonic distortion in power systems,” Eng. Licentiate Thesis, Chalmers Univ. Technol., Gothenburg, Sweden, 2001.

[27] F. C. De La Rosa, *Harmonics and Power Systems*. New York, NY, USA: Taylor & Francis, 2006.

[28] C. Venkatesh, D. Srikanth Kumar, D. V. S. S. Siva Sarma, and M. Sydulu, “Modelling of nonlinear loads and estimation of harmonics in industrial distribution system,” in *Proc. 15th Nat. Power Syst. Conf.*, Dec. 2008, pp. 592–597.

[29] C. Batard, F. Poitiers, C. Millet, and N. Ginot, “Simulation of power converters using matlab-simulink,” *MATLAB: A Fundamental Tool for Scientific Computing and Engineering Applications*, vol. 1, Vasilios Katsikis, Ed. Rijeka, Croatia: InTech, 2012.

[30] R. G. Ellis and P. Eng, *Power System Harmonics—A Reference Guide to Causes, Effects and Corrective Measures*. ON, Canada: Rockwell Int. Corp., 2001.

[31] R. Visintini, “Rectifiers,” in *CAS CERN Accelerator School Specialized Course on Power Converters*, Brandt Daniel, Ed. Geneva, Switzerland: CERN, 2006, pp. 133–183.

[32] National Programme on Technology Enhanced Learning, “Operation and analysis of the three phase fully controlled bridge converter,” 2015. [Online]. Available: http://www.nptel.ac.in/courses/ 108105066/13. Accessed on: Aug. 21, 2015.

[33] N. H. Asmar, *Partial Differential Equations With Fourier Series and Boundary Value Problems*, 2nd ed. Upper Saddle River, NJ, USA: Pearson Education, Inc., 2005.

[34] P. Duhamel and M. Vetterli, “Fast fourier transforms: A tutorial review and a state of the art (Invited paper),” *Signal Process.*, vol. 19, pp. 255–299, Apr. 1990.

[35] H. Akagi, Y. Kanazawa, and A. Nabae, “Instantaneous reactive power compensators comprising switching devices without energy storage components,” *IEEE Trans. Ind. Appl.*, vol. IA-20, no. 3, pp. 625–630, May 1984.

[36] *IEEE Recommended Practices and Requirements for Harmonic Control in Electrical Power Systems*, IEEE Std 519-2014, 2014.

[37] L. Wang, C. S. Lam, M. C. Wong, N. Y. Dai, K. W. Lao, and C. K. Wong, “Non-linear adaptive hysteresis band pulsewidth modulation control for hybrid active power filters to reduce switching loss,” *IET Power Electron.*, vol. 8, no. 11, pp. 2156–2167, Nov. 2015.

Chi-Seng Lam (S’04–M’12–SM’16) received the B.Sc., M.Sc., and Ph.D. degrees in electrical and electronics engineering from the University of Macau (UM), Macao, China, in 2003, 2006, and 2012, respectively.

From 2006 to 2009, he was an E&M Engineer in UM. In 2009, he simultaneously worked as a Laboratory Technician and started to work toward the Ph.D. degree, and completed the Ph.D. degree within 3 years. In 2013, he was a Postdoctoral Fellow in The Hong Kong Polytechnic University, Hong Kong, China. He is currently an Assistant Professor in the State Key Laboratory of Analog and Mixed-Signal VLSI, UM. He has co-authored 2 books: *Design and Control of Hybrid Active Power Filters* (Springer, 2014) and *Parallel Power Electronics Filters in Three-phase Four-wire Systems - Principle, Control and Design* (Springer, 2016), 1 US patent, 2 Chinese patents, and more than 50 technical journals and conference papers. His research interests include integrated power electronics controllers, power management integrated circuits, power quality compensators, smart grid technology, renewable energy, etc.

Dr. Lam received the Macao Science and Technology Invention Award (Third-Class) and the R&D Award for Postgraduates (Ph.D.) in 2014 and 2012, respectively. He also received the Macao Government Ph.D. Research Scholarship in 2009–2012, the Macao Foundation Postgraduate Research Scholarship in 2003–2005, and the 3rd RIUPEEEC Merit Paper Award in 2005. In 2007, 2008, and 2015, he was the GOLD Officer, a Student Branch Officer, and a Secretary of IEEE Macau Section. He is currently the Vice-Chair of IEEE Macau Section and a Secretary of IEEE Macau PES/PELS Joint Chapter. He was the Local Arrangement Chair of IEEE TENCON 2015 and ASP-DAC 2016.

Lei Wang received the B.Sc. degree in electrical and electronics engineering from the University of Macau (UM), Macao, China, in 2011, the M.Sc. degree in electronics engineering from the Hong Kong University of Science and Technology (HKUST), Hong Kong, China, in 2012, and the Ph.D. degree in electrical and computer engineering from the UM, in 2017.

Currently, he is a Postdoctoral Fellow in the Power Electronics Laboratory, UM. His research interests include power electronics, power quality and distribution flexible ac transmission system, power quality compensation, and renewable energy.

Dr. Wang received the champion award in the “Schneider Electric Energy Efficiency Cup,” Hong Kong, 2011.

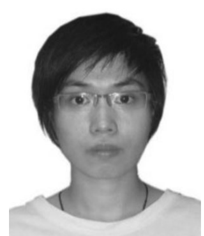

Sut-Ian Ho received the B.Sc. degree in electrical and computer systems engineering from Monash University, Victoria, Australia, in 2007, and the M.Sc. degree in electrical and computer engineering from the University of Macau (UM), Macao, China, in 2016.

From 2015 to 2016, she joined the Power Electronics Laboratory, UM, as a Part-Time Master Student. Her research interests include distribution flexible ac transmission system and power quality compensations.

Man-Chung Wong (SM’06) received the B.Sc. and M.Sc. degrees in electrical and electronics engineering from the University of Macau (UM), Macao, China, in 1993 and 1997, respectively, and the Ph.D. degree in electrical engineering from Tsinghua University, Beijing, China, in 2003.

He was a Visiting Fellow in Cambridge University, Cambridge, U.K., in 2014. He is currently an Associate Professor in the Department of Electrical and Computer Engineering, UM. He has co-authored 2 Springer books, more than 100 journal and conference papers, and 6 patents (China and USA). Recently, an industrial power filter platform was developed and installed in a practical power system based on his research results. His research interests include power electronics converters, pulse with modulation, active power filters, hybrid active power filters, and hybrid power quality compensator for a high-speed railway power supply system.

Dr. Wong received the Macao Young Scientific Award from the Macau International Research Institute in 2000, the Young Scholar Award of UM in 2001, the Second Prize for Tsinghua University Excellent Ph.D. Thesis Award in 2003, and the Macao Science and Technology Invention Award (Third-Class) in 2012 and 2014. He supervised several students to receive merit paper awards in conferences and champions in student project competitions. He was several conference committee member and the General Chair of IEEE TENCON 2015 in Macau. In 2014–2015, he was the IEEE Macau Section Chair. Recently, he is a North Representative of IEEE Region 10 Power and Energy Society and the IEEE Macau PES/PELS Joint Chapter Chair.